Int. J. Electrochem. Sci., 17 **(2022)** Article Number: 22043, doi: 10.20964/2022.04.17

International Journal of ELECTROCHEMICAL SCIENCE
www.electrochemsci.org

Corrosion Resistance Mechanism of Mica/Epoxy Coatings with Different Mica Contents in a CO_2-Cl^- System

Shidong Zhu[1,], Pan Dong[1], Xiaobo Zhang[2], Chengzheng Li[3], Xiao Hu[4], Anqing Fu[5], Shaohua Song[1], Ziwen Wang[1]*

[1] School of Materials Science and Engineering, Xi'an Shiyou University, Xi'an 710065, China;
[2] 11th Oil Production Plant of PetroChina Changqing Oilfield Company, Longdong Production Command Center, Qingyang 745000, China;
[3] Oilfield Development Division PetroChina Changqing Oilfield Company, Xi'an 710018, China;
[4] 2nd oil Production Plant, Petro China Changqing Oilfield Company, Qingyang 745100, China;
[5] State Key Laboratory for Performance and Structure Safety of Petroleum Tubular Goods and Equipment Materials of CNPC Tubular Goods Research Institute, Xi'an 710077, China.
[*]E-mail: zhusdxt@126.com

Received: 1 October 2021 / *Accepted:* 24 January 2022 / *Published:* 4 March 2022

With the development of deeper oil and gas reservoirs, the service environment for tubings applied for oil and gas transport is getting worse, and the requirements for the corrosion protection levels of tubings and casings have become more stringent. As a result, a heavy-duty coating was applied. Mica, often used as a filler in anticorrosive coatings, has good heat resistance, (electro)chemical corrosion resistance and electrical insulating properties, which can increase the corrosion resistance of polymer-based coatings. In this paper, the mica was first modified, and then the thermal stability of the resultant mica/epoxy coating was analysed by a thermogravimetric analyser. The service environment of the coating was simulated by a high-temperature autoclave, the electrochemical characteristics of the coating were studied using an electrochemical workstation assisted by three electrodes, and the coating's surface characteristics were observed by electron scanning microscopy. The results showed that the modified mica was successfully grafted with the coupling agent KH-550, which enhanced the stability of the mica in the epoxy coating. The thermal stability of the mica/epoxy coating first increased and then decreased with increasing mica content, and the thermal stability was best for the mica/epoxy coating containing 35 wt% mica. The addition of mica effectively slowed the diffusion rate of the corrosive medium through the coating in a CO_2-Cl^- system (the diffusion coefficient was reduced by an order of magnitude), improved the corrosion resistance of the coating, and prolonged the protective time of the coating towards the metal matrix. The protective performance of the coating also increased first and then decreased with increasing mica content, and the mica/epoxy coating prepared with 35 wt% mica had the best protective performance. Furthermore, combined with information about the contact angle, water absorption characteristics and adhesion properties of the composite coating, it was found that the internal diffusion rate of the medium through the coating decreased, and there was a negative correlation between water absorption kinetics and corrosion kinetics. Finally, a corrosion resistance mechanism for the mica/epoxy coating was proposed to provide theoretical support for the development of new heavy corrosion coatings.

Keywords: Epoxy resin; Mica; Coating; Corrosion resistance; Electrochemical characteristics

1. INTRODUCTION

Corrosive media, such as those containing CO_2 and Cl^-, are often used during the extraction and transport of oil and gas; therefore, the metallic pipes applied inevitably suffer from severe corrosion, and corrosion costs are continually increasing [1]. According to statistics, the oil industry in China consumes approximately 1 billion yuan of oil country tubular goods (OCTG) each year, mostly due to the prevalence of corrosion [2-3]. This situation forces the oil industry to enhance the anti-corrosion grades of OCTG and to put forward more stringent requirements for their protection.

To effectively address the ready corrodibility of carbon steel, current methods mainly include the selection of corrosion resistant materials, coatings, surface modifications and corrosion inhibitors [4]. Among these methods, the application of a (heavy anti-corrosion) coating is the most efficient and economical method. Commonly used epoxy resins achieve good adhesion with the metal matrix and resist water, and they have other favourable properties because they contain hydroxyl, epoxy, ether and other groups [5-6]. Furthermore, the high strength, high elastic modulus, strong bonding capacity and excellent chemical stability of epoxy resins often make them function as anticorrosive coatings. However, their application is limited by their brittleness, sensitivity to microcracks, low impact toughness and poor fatigue performance [7]. To further improve their corrosion resistance, the nature of the coating can be changed, but this method is difficult to implement. Therefore, researchers have shifted their focus to the addition of fillers.

A filler, as a dispersed phase, can be uniformly distributed over the entire anti-corrosion coating after the corresponding treatment process, which can reduce the internal stress of the coating during solidification, reduce its expansion coefficient, and improve its wear resistance, hardness, adhesion and flexibility to improve its corrosion resistance. Many relevant studies have pointed out that the addition of fillers increases the physical protective barrier of epoxy resins and prolongs the time required for corrosive media penetration to the metal matrix through the primers [8]. Furthermore, the addition of mica improves the impermeability of the coating to corrosive media by one order of magnitude [9] and increases the Young's modulus of HDPE (high-density polyethylene) composites [10].

The dispersion density of the filler in the coating varies with the content of the filler, which directly affects the effects of the filler in the coating and changes the compactness of the coating, which then affects the corrosion resistance of the coating. Shirehjini et al. found that adding 1 wt% clay nanoparticles enhanced the dispersion of clay in the coating, thereby improving the corrosion resistance of the coating. However, the addition of more than 1 wt% clay nanoparticles reduced the long-term protective properties of the coating [11]. Ghasemi-Kahrizsangi et al. found that the addition of 0.75 wt% carbon black prevented the diffusion of iron ions and water molecules, and the corrosion resistance of the epoxy resin matrix coating was improved [12]. Therefore, the proper addition of fillers is an effective method to improve the corrosion resistance of the coatings [13]. However, there are relatively few studies on the influence of mica content on the corrosion resistance of epoxy resins.

Previous studies have found that $800^{\#}$ mica has good dispersion in epoxy coatings. Therefore, different contents (20 wt%, 25 wt%, 30 wt%, 35 wt%, and 40 wt%) of $800^{\#}$ mica were added to an

epoxy coating, and the influence of mica content on the corrosion resistance of heavy-duty corrosion coatings was investigated to provide a theoretical basis for the development of new heavy anti-corrosion coatings.

2. EXPERIMENTAL

2.1 Coating samples preparation

2.1.1 Mica/epoxy coatings preparation

In this experiment, epoxy resin (E-08) was used as the base material, polyether amine (D230) was used as the curing agent, and modified mica was used as the filler. Different modified mica contents (20 wt%, 25 wt%, 30 wt%, 35 wt% and 40 wt%) were added to E-08. Finally, the modified mica was uniformly sprayed on N80 carbon steel (with good mechanical stability and economic feasibility [14-15]), and the coating thickness was 200±10 μm.

2.1.2 Free film preparation

The prepared coating was poured into a mould of dimensions 20 mm × 20 mm × 2 mm. To obtain a dense free film without defects, the coating was fully stirred and vacuumed before pouring to ensure that there were no pores or residual bubbles in the free film. The mould was solidified at a constant temperature of 80 °C for 24 h and then placed at room temperature for 3 days. After the free film had completely solidified, it was carefully removed from the mould and placed in a drying oven for testing. An epoxy varnish-free film and mica/epoxy-free film were prepared by the above method for water absorption tests.

2.2 Thermal stability

The thermal stability of the coating was measured by an STA7000 thermal gravimetric analyser. A small amount of sample was weighed with an electronic balance, and its thermal stability was analysed by a thermogravimetric analyser. The experiment was carried out in a N_2 atmosphere. The flow rate of N_2 was set to 20 mL/min, the furnace temperature was raised from room temperature to 800 °C, and the heating rate was 20 °C/min.

2.3 Investigation of corrosion resistance

2.3.1 Simulated immersion test

A high-temperature and high-pressure reactor was used to better simulate the downhole operating environment. The experimental temperature was 120 °C, the total pressure was 15 MPa (CO_2 partial pressure 5 MPa), the experimental time was set to 120 h and 240 h, and the medium was a 10% NaCl solution.

2.3.2 Electrochemical test

The electrochemical test sample size was Ø20 mm × 3 mm. The electrochemical test sample was welded with copper wire and packaged with resin, with a reserved surface area of 3.14 cm^2. In this electrochemical test, the open circuit potential, electrochemical impedance and the polarization curve of the coating were tested by a Princeton electrochemical workstation (P4000). A three-electrode system was used. The auxiliary electrode was a platinum electrode, the reference electrode was a saturated calomel electrode (SCE), and the working electrode was coated with a steel sheet. The experiment was carried out under normal pressures. The working electrode was immersed in a 10% NaCl solution, the temperature was 80 °C, the total pressure was 5 MPa (partial pressure of CO_2 was 3 MPa), and the immersion times were 60 h, 120 h and 240 h. N_2 gas was introduced for 2 h before the deoxygenation test, and the CO_2 saturation of the solution was maintained during the test. The impedance test frequency range was 10^5 Hz ~ 10^{-2} Hz. When the polarization curve was tested, the potential scanning interval was -0.5 V ~ 0.5 V, and the scanning rate was 0.5 mV/s.

2.4 Physical and chemical properties test

2.4.1 Contact angle

A JC2000D1 contact angle tester was used to test the coating contact angle. A needle of 0.725 mm was used, and the droplet volume was 10 μL. Each sample (100 mm × 50 mm × 3 mm) was tested three times, and the average contact angle of the droplets was used as the contact angle of the coating.

2.4.2 Hydrophilia

An electronic balance (precision of 0.0001 g) was used to weigh the samples (100 mm × 50 mm × 3 mm). The test method was as follows: the free film before immersion was weighed and recorded as the initial weight m_0. Subsequently, after immersion, the free film was placed in an autoclave at 80 °C and a total pressure of 5 MPa (the partial pressure of CO_2 was 3 MPa) for different times (0 h, 24 h, 48 h….240 h). Filter paper was used to quickly wipe the solution from the surface of the sample for weighing as m_t. Three parallel samples were measured in each group, and the mean value was used as the final result. The water absorption rate was calculated according to Equation (1):

$$Qt=\frac{m_t-m_0}{m_0}\times 100\% \quad (1)$$

where Q_t represents the water absorption at time t, m_t represents the weight of the free membrane at time *t*, and m_0 represents the initial weight of the free membrane.

2.4.3 Adhesion

The adhesion test temperature was set to 80 ℃, the total pressure was 5 MPa (the partial pressure of CO_2 was 3 MPa), and the immersion times were 60 h, 120 h, and 240 h. The test was carried out in accordance with GB. T5210-2006 (《Paint and varnish - pull-out adhesion test》). Six tests were conducted on each group of samples (100 mm × 50 mm × 3 mm), and the maximum test

value was taken as the adhesion between the coating and metal (unit: MPa).

3. RESULT AND DISCUSSION

3.1 Mica modification

The infrared absorption spectra are shown in Figure 1. The absorption peak for the -Si-O-Si- stretching vibration appeared near 1028 cm^{-1}, and the absorption peak for the stretching vibration of -Al-O was near 450 cm^{-1}. The stretching vibration absorption peak for -Si-OH was near 3620 cm^{-1}, which was significantly lower than that of unmodified mica, while the absorption peak characteristics in the other fingerprint areas were essentially the same. This was due to the reaction between the -Si-OH on the mica surface and the -Si-OH formed after hydrolysis of KH-550, forming a -Si-O-Si- absorption peak. At the same time, the modified mica had a weak absorption peak near 2972 cm^{-1}, which mainly arose from the vibration absorption of coupling agents $-CH_2$ and $-CH_3$. Thus, the mica surface was successfully grafted with coupling agent KH-550.

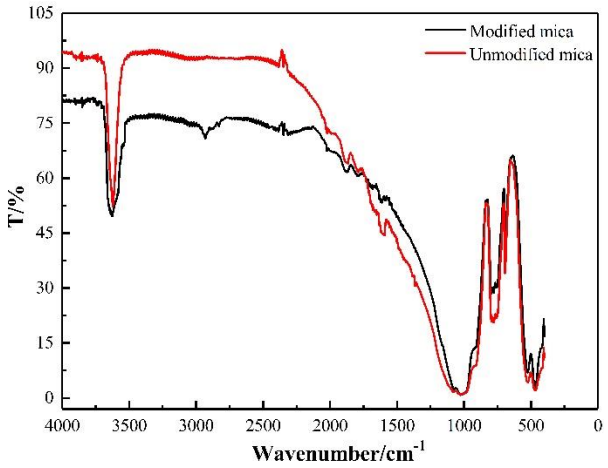

Figure 1. Infrared absorption spectra of mica before and after modification.

At present, there are four main types of modification technologies [16]: ① coupling agent modification; ② esterification reaction modification; ③ polymer grafting modification; and mechanochemical grafting and encapsulation modification. The Si-O-Si bond in mica will be broken and form Si-O groups when the mica is crushed and refined, and the Si-O group will be hydrolysed to Si-OH. When mica is modified by the coupling agent, the methoxy group and ethoxy group on the coupling agent first generate silanol through the hydrolysis reaction. Silanol reacts with -OH on the surface of mica to generate hydrogen bonds and shrinks to synthesize -Si-O-M covalent bonds (M is the silicon, aluminium and potassium in mica). At the same time, the silane coupling agent hydrolyses the silanol so the groups are able to associate with each other and connect to form a networked film structure covering the surface of the mica, which makes the surface of the mica organic. Therefore, a coupling agent was used to modify the surface of the mica as the filler to enhance its dispersion in the epoxy resin and eliminate the effects associated with the poor compatibility between mica and the

polymer.

3.2 Thermal stability

Figure 2 shows the TGA curves of the epoxy varnish coating and mica/epoxy coating with different mica contents. As seen from Figure 2, the thermal stability of the mica/epoxy coating with different mica contents was higher than that of the epoxy varnish coating. The reason was that the special lamellar structure of the mica prevented heat from penetrating into the medium. At the same time, it could also prevent the diffusion of thermal degradation products to the outside of the coating by the formation of the organic chain space intervals, limiting their movement when the coating is heated and improving the thermal stability of the coating [17].

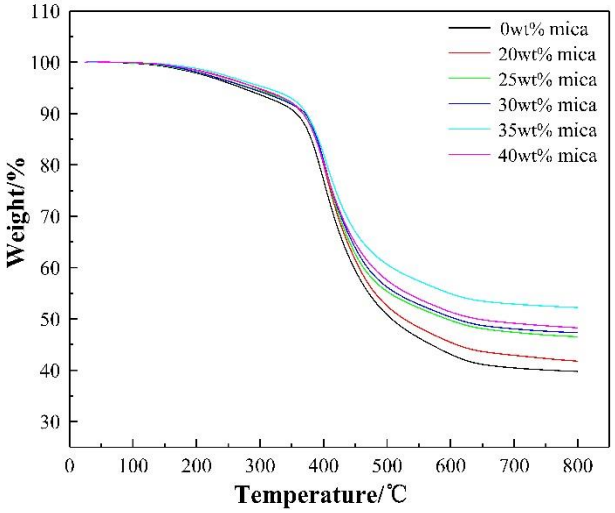

Figure 2. Thermal weight loss curves of the epoxy varnish coating and mica/epoxy coatings with different mica contents (the flow rate of N_2 was 20 mL/min, and the temperature of the furnace was increased from room temperature to 800 ℃ at a rate of 20 ℃/min).

When the weight loss rate of the epoxy varnish coating was 10 wt%, 20 wt% and 45 wt%, the corresponding temperatures were 357 °C, 393 °C and 471 °C, respectively. The corresponding temperatures of the 20 wt% mica/epoxy coating were 367 °C, 400 °C and 481 °C; the 25 wt% mica/epoxy coatings were 368 °C, 401 °C and 504 °C; the 30 wt% mica/epoxy coatings were 371 °C, 402 °C and 514 °C; the 35 wt% mica/epoxy coatings were 373 °C, 405 °C and 598 °C; the 40 wt% mica/epoxy coatings were 367 °C, 401 °C and 532 °C. In summary, the thermal stability of the coating first increased and then decreased with decreasing mica contents, and the thermal stability of the mica/epoxy coating prepared at 35 wt% addition was the best.

3.3 Surface characteristics after immersion

Figure 3 and Figure 4 show the surface changes of the epoxy varnish coating and mica/epoxy coating with different mica contents before and after high-temperature and high-pressure corrosion

tests, respectively. The surfaces of the epoxy varnish coating and the mica/epoxy coating with different contents were smooth and without defects before the immersion test, and the surface colour was black and bright with full lustre.

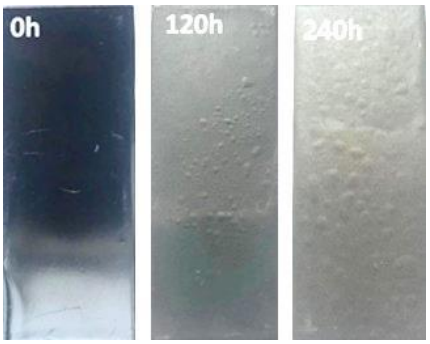

Figure 3. Macromorphology of the epoxy varnish coating in the high-temperature and high-pressure corrosion tests (The experimental temperature was 120 °C, the total pressure was 15 MPa (the partial pressure of CO_2 was 5 MPa), the experimental time was set to 120 h and 240 h, and the medium was a 10% NaCl solution.).

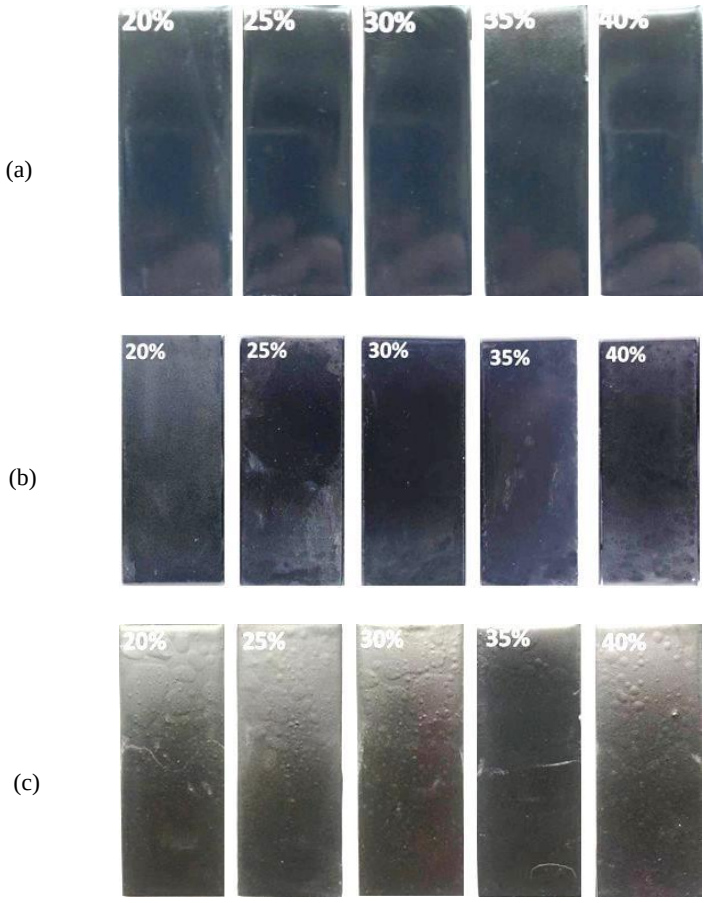

Figure 4. Macromorphology of different contents of mica/epoxy coatings in the high-temperature and high-pressure corrosion tests: (a) 0 h immersion, (b) 120 h immersion, and (c) 240 h immersion (the experimental temperature was 120 °C, the total pressure was 15 MPa (the partial pressure of CO_2 was 5 MPa), the experimental time was set to 120 h and 240 h, and the medium was a 10% NaCl solution).

After immersion for 120 h, a small part of the epoxy varnish coating blistered, and the coating colour was grey and the coating had lost its lustre. This might be because the corrosive medium had penetrated into the coating through some pores, eroding the metal matrix. However, there were no defects, such as foaming and cracks, in any of the mica/epoxy coating groups. This was because, although the corrosive medium had infiltrated the coating, the addition of mica prolonged the time required for the corrosive medium to penetrate to the interior of the coating [8]. The corrosion medium did not reach the interface between the coating and the metal, and the coating still had the ability to isolate the corrosion medium and had good adhesion with the metal matrix. In addition, the colour change of the mica/epoxy coating prepared with 35 wt% mica was the lowest in the same group.

After immersion for 240 h, there was a large area of intensive foaming in the epoxy varnish coating. In all the mica/epoxy coating groups, the coating surface exhibited a foaming phenomenon for the addition of 20 wt%, 25 wt%, 30 wt% and 40 wt% mica. However, there were no surface defects for 35 wt% mica. Therefore, with increasing mica content, the protective performance of the coating first increased and then decreased. Therefore, with the addition of mica to the coating and the increase in mica content, the diffusion path of the corrosive medium became more tortuous [18-19]; thus, the time required for the corrosive medium to penetrate the coating to corrode the metal matrix was prolonged. When the additive amount exceeded 35 wt%, the dispersion of the mica in the resin decreased, and an agglomeration phenomenon occurred [20]. The number of internal defects in the coating increased, which weakened the shielding ability of the coating towards the corrosive medium.

3.4 Electrochemical characteristics

The coating could be tracked and measured over a long period by electrochemical testing. According to the thermal stability of the coating and the corrosion morphology of the high-temperature and high-pressure immersion, the coating prepared with 35 wt% mica performed the best amongst the epoxy coatings with different mica contents. Some researchers tested the electrochemical impedance spectrum of epoxy acrylate composite coatings after adding mica and believed that the optimal mica content was achieved when the gaps between the pigment particles were occupied by the polymer; this enhanced the coating's shielding performance against the corrosive medium [21]. Therefore, the epoxy varnish coating and 35 wt% mica/epoxy coating were selected for further investigation, and the corrosion resistance of the coating was investigated by an electrochemical detection method.

1）Open circuit potential

Figure 5 shows the change in the open circuit potential of the epoxy varnish coating and the 35 wt% mica/epoxy coating in real time. The OCP value of the coating changed with the extension of immersion time, which reflected a change in the internal protection mechanism of the coating [22].

As seen from Figure 5, the open circuit potential of the epoxy varnish coating and the 35 wt% mica/epoxy coating gradually decreased with the extension of immersion time. Over the entire immersion process, it was clear that the open circuit potential of the two coatings had a sudden decrease and subsequent increase. The open circuit potential of the epoxy varnish coating decreased from 0.30 V to -0.36 V over the range of 9 h-12 h immersion times and then increased to 0.27 V with an increasing immersion period. However, the potential of the 35 wt% mica/epoxy coating decreased

from 0.29 V to -0.31 V over the range of 88 h-96 h immersion times and then increased to 0.22 V with an increasing immersion period.

The rapid negative shift in the open circuit potential indicated that water seeped into the coating/metal interface and began to corrode the metal matrix. However, with increasing immersion time, the corrosion potential began to increase, mainly because, as the corrosion progressed, the corrosive medium "plunged into" the coating/metal interface in water. Anodic dissolution of the metal under the coating and cathodic stripping of the coating occurred. The exposed area of the metal increased, which led to an increase in the area and was beneficial to the cathodic reaction, namely, increasing the area ratio of the cathode to anode and making the corrosion potential more positive [23]. During this period, the aqueous solution gradually penetrated into the coating and reached the coating/metal bonding site through numerous microchannels. The corrosion medium continually penetrated, and corrosion occurred at the coating/metal interface.

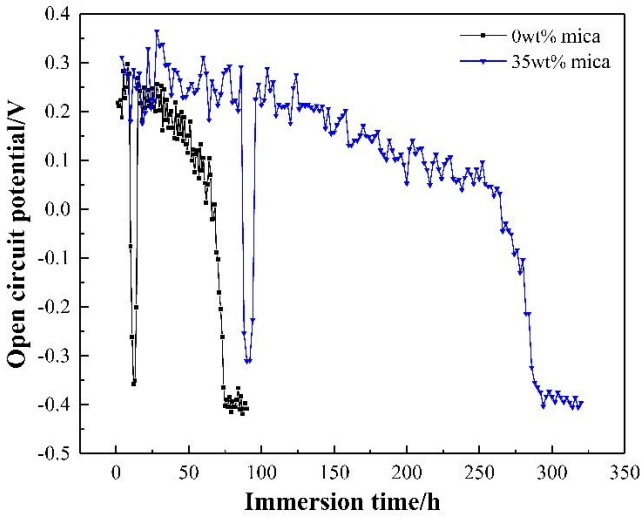

Figure 5. Relationship curve between open circuit potential and immersion time of coating (The medium was a 10% NaCl solution, the temperature was 80 °C, the total pressure was 5 MPa (Partial pressure of CO_2 was 3 MPa), and the immersion time was 60 h, 120 h and 240 h).

During the mid-range for immersion times, the open circuit potential of the two coatings gradually decreased, indicating that the reactions of the cathode and anode were relatively balanced during the corrosion process, and the coatings were slowly destroyed. However, in the later stages of immersion, the open circuit potential of the epoxy varnish coating decreased rapidly and stabilized to -0.41 V after 66 h. However, the open circuit potential of the 35 wt% mica/epoxy coating began to decrease rapidly and stabilized at -0.39 V after 274 h, indicating that the protective performance of the coating was essentially stable during the later stages of immersion, but its potential during the same time was higher than that of the N80 carbon steel matrix [24].

The change in the open circuit potential of the epoxy varnish coating was similar to that of the 35 wt% mica/epoxy coating, reflecting the approximate time for coating infiltration and the corrosive electrochemical reaction. The corrosion initiation time for the 35 wt% mica/epoxy coating in each

stage was later than that of the epoxy varnish coating, indicating that the weakening of corrosion resistance was relatively slow and the protective performance was better.

2）Alternating-current impedance

Alternating-current impedance is the most commonly used nondestructive testing technique used to study organic coatings [25-26], and it can evaluate the evolution process for the anticorrosive properties of organic anticorrosive coatings. Figure 6 shows the EIS of the epoxy varnish coating immersed for different times. As shown in the figure, the capacitive arc radius of the epoxy varnish coating gradually decreased with increasing immersion time. Generally, the capacitance arc of the high-frequency region is used to characterize the protective properties of a coating [27]: The larger the arc radius is, the greater the resistance of the coating and the better the protection performance. The smaller the coating capacitance is, the more significant the effect of preventing the corrosion medium from passing through the coating.

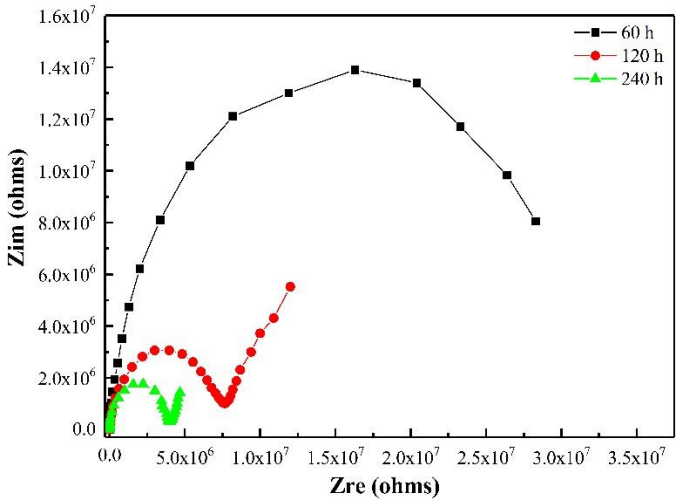

Figure 6. Nyquist diagram of epoxy varnish coating immersed for different times (the medium was a 10% NaCl solution, the temperature was 80 °C, the total pressure was 5 MPa (partial pressure of CO_2 was 3 MPa), and the immersion time was 60 h, 120 h and 240 h).

The impedance data were fitted with a ZsimpWin software, and its equivalent circuit diagram is shown in Figure 7. The fitting results are shown in Table 1, in which R_s represents solution resistance, C_c and R_c represent the coating capacitance and coating resistance, C_{dl} and R_{ct} represent the double layer capacitance and charge transfer resistance, and W represents Warburg diffusion resistance, which could be used to describe the diffusion process for corrosive media into the substrate through a layer of corrosion products [28]. According to the literature, the coating resistance R_c could reflect the shielding effect of the coating from a corrosive medium [29], and R_{ct} could reflect the difficulty of metal interface charge transfer and be used to evaluate the corrosion rate. It was generally believed that the higher the R_{ct} was, the more difficult the corrosion reaction be and the slower the corrosion rate would be. In contrast, the lower the R_{ct} was, the more likely the corrosion reaction would be and the faster corrosion rate would be [30].

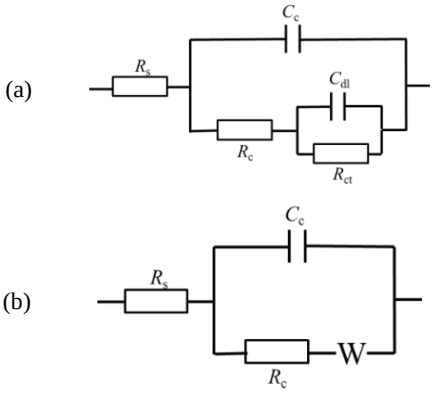

Figure 7. Equivalent circuit diagram of the coating.

Table 1. Fitting of the impedance equivalent circuit diagram of the epoxy varnish coating after immersion for different times.

Immersion time/h	R_s/Ω·cm^2	C_c/F·cm^{-2}	R_c/Ω·cm^2	C_{dl}/F·cm^{-2}	R_{ct}/Ω·cm^2	W/Ω·cm^2
60	1.585×10^{-3}	1.151×10^{-10}	6.956×10^{7}	6.244×10^{-10}	3.581×10^{7}	/
120	1.699×10^{-3}	1.451×10^{-10}	6.455×10^{6}	/	/	1.360×10^{-7}
240	3.613×10^{-2}	3.161×10^{-10}	3.715×10^{5}	/	/	1.216×10^{-6}

After immersion for 60 h, the circuit shown in Figure 7(a) was used for fitting. At this point, the coating resistance was 6.956×10^{7} Ω·cm^2. The impedance spectra showed a time constant and Warburg impedance characteristics after immersion for 120 h and 240 h, indicating that the passage of the corrosive medium into the coating was blocked; the coating resistance values were 6.455×10^{6} Ω·cm^2 and 3.715×10^{5} Ω·cm^2, respectively, according to the circuit shown in Figure 7(b).

Figure 8 shows the impedance spectra of the 35 wt% mica/epoxy coating. Figure 8 shows that all the impedances of the coating after immersion for different times exhibited double capacitance characteristics. Considering that the corrosive medium might reach the coating/metal interface and corrode the metal matrix after long-term immersion in the solution, forming corrosive microbatteries at the interface between the coating and metal, Figure 7(a) was used for fitting [31], and the fitting data are shown in Table 2. The impedance spectrum characteristics did not change with the immersion time, but the impedance value eventually decreased with the extension of immersion time.

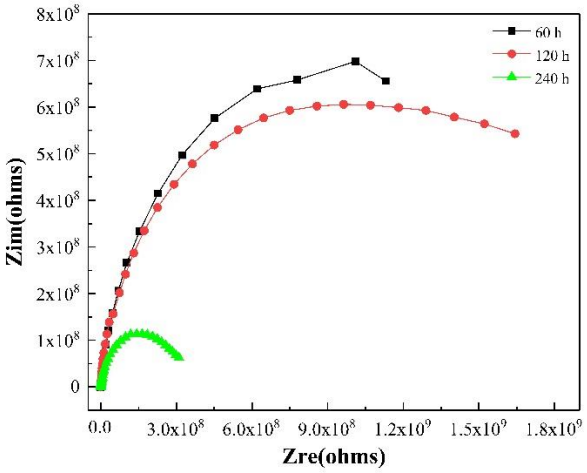

Figure 8. Nyquist diagram of the 35wt% mica/epoxy coating immersed for different times (The medium was a 10% NaCl solution, the temperature was 80 °C, the total pressure was 5 MPa (Partial pressure of CO_2 was 3 MPa), and the immersion times were 60 h, 120 h and 240 h).

Table 2. Data fitting of the impedance equivalent circuit diagram of the 35 wt% mica/epoxy coating after immersion for different times.

Immersion time/h	R_s/Ω·cm^2	C_c/F·cm^{-2}	R_c/Ω·cm^2	C_{dl}/F·cm^{-2}	R_{ct}/Ω·cm^2
60	1.220×10^{-3}	1.076×10^{-10}	1.212×10^{9}	9.984×10^{-10}	1.620×10^{9}
120	1.997×10^{-3}	2.323×10^{-10}	9.164×10^{8}	1.024×10^{-9}	1.486×10^{9}
240	2.472×10^{-3}	3.866×10^{-10}	2.637×10^{8}	6.814×10^{-9}	7.404×10^{8}

The above comparative study shows that the corrosion resistance of the 35 wt% mica/epoxy coating was stronger than that of the epoxy varnish coating for the same immersion times, indicating that the addition of mica to the coating could effectively suppress the decrease in the corrosion resistance of the coating and improve the ability of the coating to protect the metal matrix. The reason the corrosion resistance of the epoxy coating was enhanced by the addition of an optimal amount of mica filler is that it adhered better and improved protective properties of the coating [32].

3）Polarization curve

Potentiodynamic polarization curve measurements are an important means to characterize the electrode corrosion rate. The polarization curve includes a linear polarization zone, a weak polarization zone and a strong polarization zone. The *E*-log*i* of the strong polarization zone is close to a straight line and can be fitted as a linear function [33]. Figure 9 and Figure 10 show the polarization curves of the epoxy varnish coating and the 35 wt% mica/epoxy coating after immersion for different times. Table 3 and Table 4 show the fitting data for the polarization curves of the epoxy varnish coating and the 35 wt% mica/epoxy coating after immersion for different lengths of time.

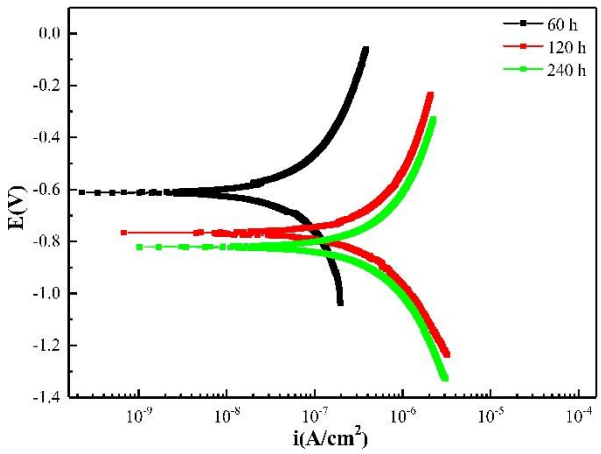

Figure 9. Polarization curve of the epoxy varnish coating after immersion for different lengths of time (the medium was a 10% NaCl solution, the temperature was 80 °C, the total pressure was 5 MPa (the partial pressure of CO_2 was 3 MPa), and the immersion times were 60 h, 120 h and 240 h).

Table 3. Polarization curve fitting data of the epoxy varnish coating after immersion for different lengths of time.

Immersion time/h	E_{corr}/V	I_{corr}/A·cm^{-2}	R_P/Ω·cm^2
60	-0.611	2.25×10^{-10}	9.04×10^{6}
120	-0.766	6.71×10^{-10}	2.12×10^{6}
240	-0.821	1.02×10^{-9}	8.96×10^{5}

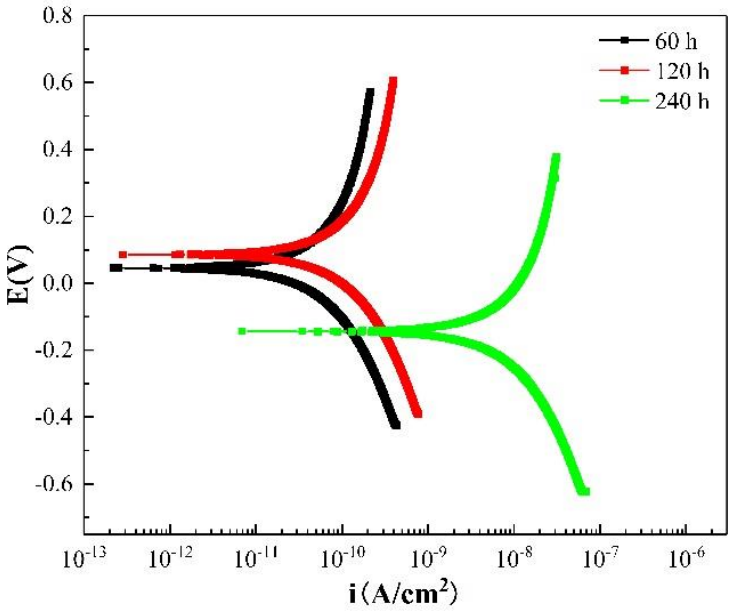

Figure 10. Polarization curve of the 35 wt% mica/epoxy coating after immersion for different lengths of time (the medium was a 10% NaCl solution, the temperature was 80 °C, the total pressure was 5 MPa (partial pressure of CO_2 was 3 MPa), and the immersion times were 60 h, 120 h and 240 h).

Table 4. Polarization curve fitting data of the 35 wt% mica/epoxy coating after immersion for different lengths of time.

Immersion time/h	E_{corr}/V	I_{corr}/A·cm^{-2}	R_p/Ω·cm^2
60	0.116	3.29×10^{-14}	5.80×10^{9}
120	0.086	2.84×10^{-13}	9.87×10^{8}
240	-0.144	6.86×10^{-12}	4.13×10^{8}

Figure 9 and Table 3 show that the self-corrosion potential E_{corr} of the epoxy varnish coating decreased with increasing immersion time, from -0.611 V to -0.821 V. The self-corrosion current I_{corr} increased gradually with increasing immersion time, from 2.25×10^{-10} A·cm^{-2} to 1.02×10^{-9} A·cm^{-2}. The polarization resistance R_p decreased gradually with increasing immersion time, from 9.04×10^{6} Ω·cm^2 to 8.96×10^{5} Ω·cm^2. The corrosion resistance of the epoxy varnish coating decreased gradually with increasing immersion time.

Figure 10 and Table 4 show that the self-corrosion potential E_{corr} of the 35 wt% mica/epoxy coating decreased with increasing immersion time from 0.116 V to -0.144 V. The self-corrosion current I_{corr} increased gradually with increasing immersion time, from 3.29×10^{-14} A·cm^{-2} to 6.86×10^{-12} A·cm^{-2}. The polarization resistance R_p decreased with increasing immersion time, from 5.80×10^{9} Ω·cm^2 to 4.13×10^{8} Ω·cm^2. The corrosion resistance of the 35 wt% mica/epoxy coating also gradually decreased with increasing immersion time.

By comparing the two coatings, it was found that the E_{corr} of the mica/epoxy coating was higher than that of the epoxy varnish coating for the same immersion periods. For example, the potential of the mica/epoxy coating increased by 0.8515 V compared with that of the epoxy varnish coating after immersion for 120 h. At the same time, the I_{corr} of the mica/epoxy coating was found to be less than that of the epoxy varnish coating. For example, the I_{corr} of the mica/epoxy coating was lower by 4 orders of magnitude compared with the epoxy varnish coating after 60 h of immersion. The higher the E_{corr} and the lower the I_{corr} are, the better the corrosion resistance of the coating [26, 34-35]. Shakoor et al. showed that, compared with a Ni-B coating, the corrosion current density of a Ni-B-SiO_2 coating decreased significantly, and the corrosion potential increased significantly, indicating that the addition of silica particles to Ni-B improved its corrosion resistance [36]. Fu et al. showed that the self-corrosion potential of a Ni-Fe-Co-P alloy coating with GO increased gradually, the self-corrosion current decreased gradually, and the corrosion resistance of the coating increased [37]. Therefore, the mica/epoxy coating prepared with 35 wt% mica had better performance for isolating corrosive media. The reason can be attributed to the modified mica being uniformly dispersed in the composite coating, which leads to the dispersion of the corrosion current and a decrease in the corrosion rate [38].

SEM analysis, which is more conducive to an in-depth and thorough analysis of the anticorrosion mechanisms of coatings, was used to analyse the morphology of the 35 wt% mica/epoxy coating [39-40]. As seen from Figure 11, the distribution of the mica in the 35 wt% mica/epoxy coating was uniform, and the gaps between the mica particles were small. Therefore, the addition of mica filled the structural pores of the EP and hindered the diffusion of the corrosive medium and its contact with the metal matrix, thereby improving the corrosion resistance of the coating [41].

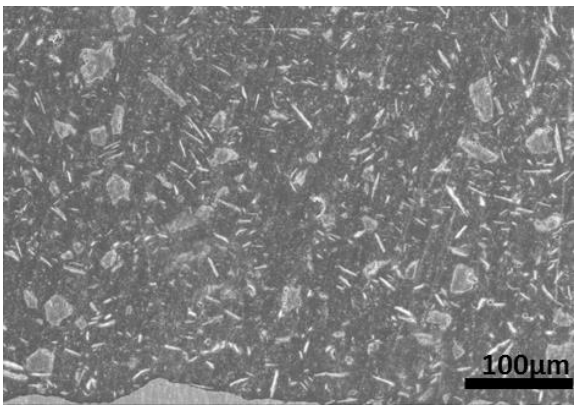

Figure 11. SEM morphology of the 35 wt% mica/epoxy coating before immersion.

3.5 Corrosion resistance mechanism

3.5.1 Contact angle

The hydrophobicity of a coating is an important criterion to determine its corrosion resistance. The hydrophobic property of a coating can reduce the adhesion and permeability of water molecules to the coating surface to effectively reduce or prevent the electrochemical corrosion of the metal matrix. The better the hydrophobicity of the coating is, the better the corrosion resistance [42-43]. Figure 12 shows the contact angle diagram for the two coatings, and Table 5 shows the contact angle of the two coatings.

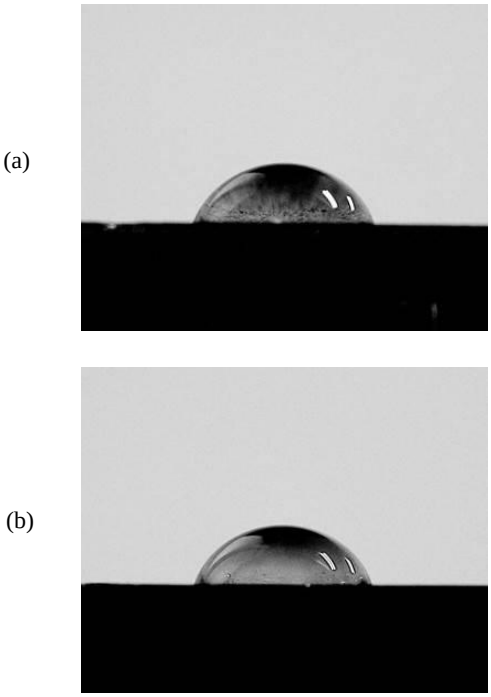

Figure 12. Contact angle test of the coatings. (a) Epoxy varnish coating, (b) 35 wt% mica/epoxy coating.

Table 5. Contact angle of the coatings.

Sample	Contact angle/°
Epoxy varnish coating	70.4
35wt% mica/epoxy coating	72.8

Figure 12 and Table 5 show that the contact angles of the epoxy varnish coating and mica/epoxy coating were small. The contact angle of the coating did not change significantly with the addition of mica. It could be inferred that the mica/epoxy coating did not produce a lower medium permeability by reducing the contact surface between the corrosive medium and the coating surface, which would result in a slower diffusion rate for the corrosive medium in the coating. However, the addition of mica had a small effect, which could be attributed to a wettability problem. The contact angle of the mica/epoxy coating was slightly larger than that of the epoxy varnish coating, indicating that the addition of mica could lead to a slightly lower wettability, which could suppress the passage of the corrosive medium and reduce the erosion effect of the matrix.

3.5.2 Hydrophilia and water absorption kinetics

Figure 13 shows the water absorption curves of the epoxy varnish coating and the mica/epoxy coating. The figure shows that over the entire immersion period, the variation in the water absorption characteristics of the two coatings were composed of two stages: a rapid absorption stage and a saturation stage.

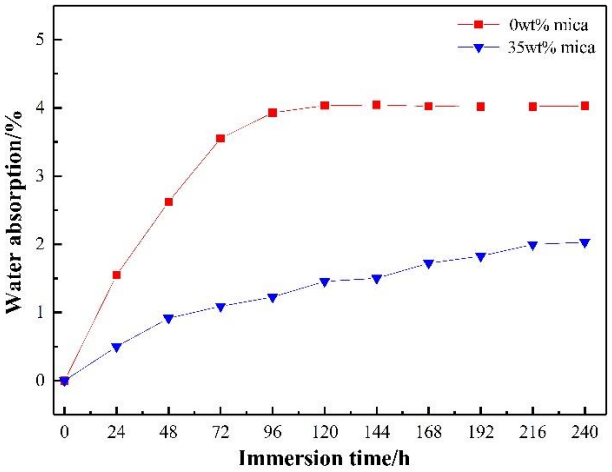

Figure 13. Water absorption rate curves of the epoxy varnish coating and the mica/epoxy coating (The temperature was 80 °C, the total pressure was 5 MPa (Partial pressure of CO_2 was 3 MPa), and the immersion times were 0 h, 24 h, 48 h … 240 h).

During the rapid absorption stage, the water absorption rate of all the tested samples increased rapidly, but the water absorption rate of the 35 wt% mica/epoxy coating was less than that of the epoxy varnish coating for the same immersion times. In addition, the epoxy varnish coating reached a saturation state after approximately 120 h of rapid water absorption. However, the 35 wt% mica/epoxy

coating reached saturation slowly after 216 h of immersion. At approximately 240 h of immersion time, the water absorption rate of the epoxy varnish coating was 4.03%, while that of the 35 wt% mica/epoxy coating was 2.03%. At this time, the water absorption rate of the 35 wt% mica/epoxy coating was approximately two times lower than that of the epoxy varnish coating, indicating that it had a strong shielding effect against corrosive media.

The transmission mechanism for water entering the epoxy varnish coating and the 35 wt% mica/epoxy coating under constant pressure is discussed to further understand the transmission process for water entering the coating and the difference in permeability resistance between the two coatings. The research results show that, assuming solution diffusion in the coating was close to ideal Fickian diffusion [44-48], a relationship between the coating's water absorption and time could be obtained:

$$\frac{M_t}{M_\infty}=1-\frac{8}{\pi^2}\sum_{n=0}^{\infty}\frac{1}{(2n+1)^2}\exp[\frac{-(2n+1)^2D\pi^2}{L^2}t] \quad (2)$$

M_t and M_∞ are the water absorption of the coating at time t and saturation, L is the thickness of the coating, and D is the diffusion coefficient of water. In the early stages of immersion, Equation (2) has the following approximate equation:

$$\frac{M_t}{M_\infty}=\frac{4}{l}\sqrt{\frac{D}{\pi}}\cdot\sqrt{t} \quad (3)$$

The amount of water absorbed by the coating was proportional to the square root of time. The diffusion coefficient of water in the coating could be obtained by using this equation to characterize the diffusion behaviour of water in the coating. The relationship between the coating's water absorption and time over a relatively short time can be expressed as:

$$M_t=Kt^n \quad (4)$$

K is a constant, n is a constant and n>0. If n=0.5, diffusion conforms to the ideal Fick's diffusion law. When n≠0.5, diffusion is of the non-Fickian form, where n=1 is type II diffusion, indicating that the water absorption M_t of the coating is linear with time t. The type of diffusion process occurring can be determined by the value of n.

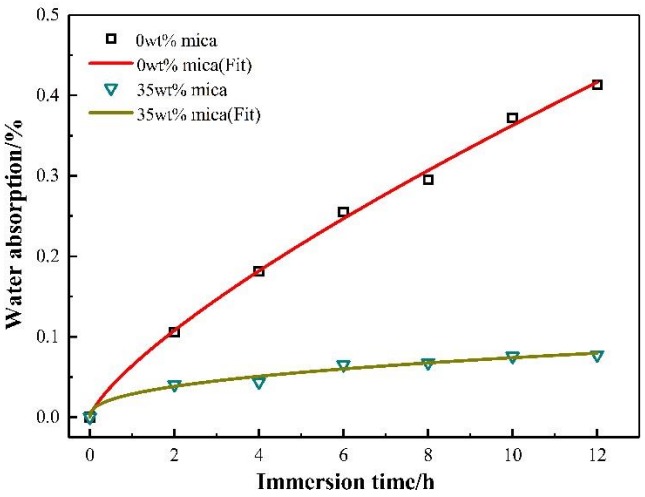

Figure 14. Water absorption kinetics curves for the coatings at the initial immersion stage (constant pressure).

Table 6. Nonlinear fitting results and diffusion coefficients of the solution through the coatings.

Sample	Pressure/MPa	A	B	Diffusion coefficient D/$cm^2.s^{-1}$
Epoxy varnish coating	5	0.06262	0.86192	6.873×10^{8}
35wt% mica/epoxy coating		0.02442	0.54675	5.306×10^{7}

Figure 13 shows that the water absorption of the coatings was in a rapid absorption stage at the beginning of immersion. Therefore, the water absorption kinetics curves of the epoxy varnish coating and the 35 wt% mica/epoxy coating were nonlinearly fitted by a $y=Ax^B$-type equation (Figure 14), and the corresponding diffusion coefficients were calculated according to Equation (3). The results are shown in Table 6.

The results showed that the diffusion coefficient of the epoxy varnish coating was 6.873×10^8 $cm^2.s^{-1}$, and the diffusion coefficient of the 35 wt% mica/epoxy coating was 5.306×10^7 $cm^2.s^{-1}$. Clearly, the diffusion coefficient of the coating decreased by slightly more than one order of magnitude after adding mica, indicating that the addition of mica to the coating could make the diffusion channels in the corrosion medium longer, effectively reduce the diffusion velocity of water in the coating, and prolong the protection time of the coating on the metal matrix.

3.5.3 Adhesion

The adhesion of organic coatings to substrates is mainly related to the cohesion of the organic coating and the adhesion of the coating to the substrate [49]. Adhesion can determine whether the diffusion of the corrosive medium can be effectively restricted at the interface between the coating and metal [50]. Figure 15 shows the test results for adhesion between the epoxy varnish coating and the mica/epoxy coating before and after immersion.

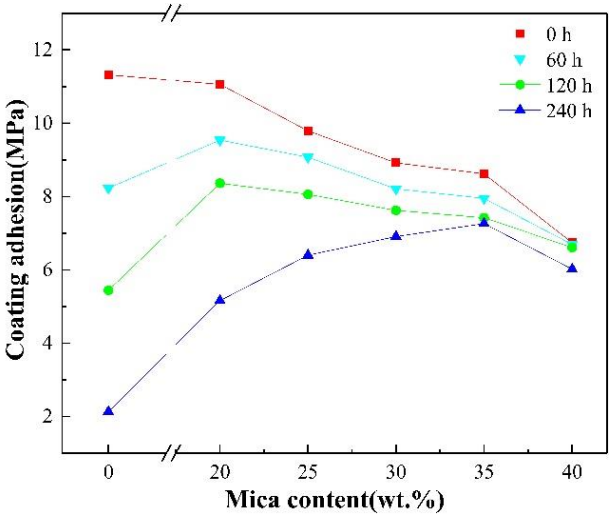

Figure 15. Change in adhesion between the epoxy varnish coating and the mica/epoxy coating before and after immersion (The temperature was 80 °C, the total pressure was 5 MPa (Partial pressure of CO_2 was 3 MPa), and the immersion times were 60 h, 120 h and 240 h).

Figure 15 shows that, before the immersion test, the adhesion of the epoxy varnish coating was greater than that of the mica/epoxy coating for all mica contents. The reason can be found in the SEM cross-sectional morphology of the 35 wt% mica/epoxy coating before immersion, as shown in Figure 11, where part of the mica appears on the metal matrix. However, there is no binding force between the mica and the metal matrix, resulting in a decrease in the contact area and adhesion between the epoxy coating and metal matrix.

At the same time, after immersion for 60 h and 120 h, the adhesion of the mica/epoxy coating decreased with increasing mica content in the epoxy coating. However, over a period of immersion for 240 h, with increasing mica content, the adhesion of the mica/epoxy coating first increased and then decreased. The maximum adhesion was 7.26 MPa at a mica content of 35 wt%.

Before the coating was immersed, with the increase in mica content in the unit volume coating, the proportion of the resin in the unit volume coating gradually decreased. When the mica content reached the limit that could be accommodated in a unit volume of the resin, the inclusion of the resin in the filler reached saturation. However, the adhesion of the coating came from the bonding between the resin and the metal matrix. The decrease in the resin ratio could be regarded as a decrease in the "glue" over a unit area of the metal matrix. At this point, the increasing mica content relative to resin would prevent the epoxy resin from covering the mica particles; therefore, the adhesion changed from a slow decline to a sharp decline in the figure.

During the coating immersion process, the corrosive medium penetrated into the coating from the surface of the coating and gradually reached the coating/metal interface to corrode the metal matrix, which reduced the adhesion between the coating and the metal matrix. The addition of mica strengthened the shielding effect of the coating against the corrosive medium. With increasing mica content, the infiltration path of the corrosion medium into the coating became more complex [18], which enhanced the impermeability of the coating. When the mica content was too low, it was difficult to construct a complex path for the infiltration of the corrosive medium into the coating. When the mica content was too high, the epoxy resin could not cover all the mica particles, which increased the number of defects in the coating and reduced the shielding performance of the coating against the corrosive medium. As a result, the metal matrix was easily corroded, resulting in a rapid reduction in coating adhesion.

As the corrosive medium penetrated the coating/metal interface, the coating gradually lost its adhesion to the substrate due to the debonding effect of water. To further analyse the interfacial fracturing of the epoxy varnish coating and the 35 wt% mica/epoxy coating, the morphology of the samples after the adhesion test was observed (Figure 16). The adhesion of the coating was measured by the adhesion of the coating to the substrate and the cohesion of the coating, and a difference in the relative strength of the two would result in different fracture forms. According to the location of the fracture of the two coatings and the size of the shedding area during the adhesion test, the fracture morphologies in adhesion could be divided into four types [23], as shown in Table 7.

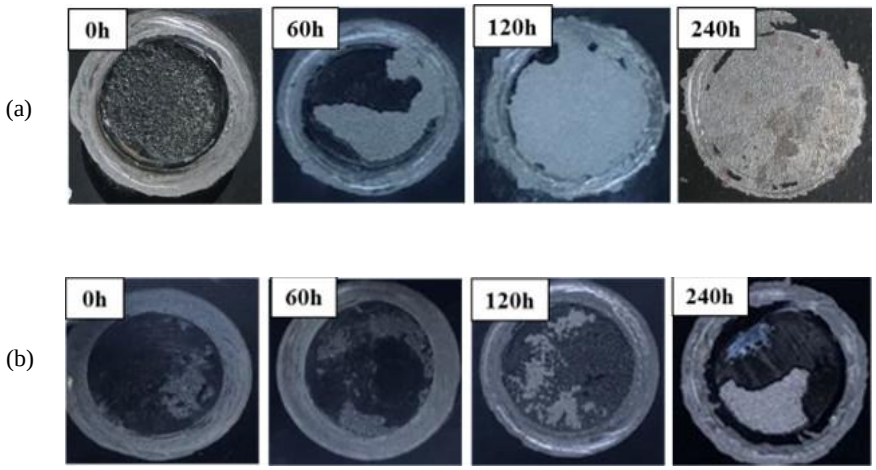

Figure 16. Fracture morphology change in adhesion fracturing before and after coating immersion tests. (a) Epoxy varnish coating, (b) 35wt% mica/epoxy coating (The temperature was 80 °C, the total pressure was 5 MPa (Partial pressure of CO_2 was 3 MPa), and the immersion times were 60 h, 120 h and 240 h).

Table 7. Fracture morphology of coating adhesion.

Cohesive fracture	The coating is fractured within the body of the coating and is partially bonded to the substrate, leaving the substrate unexposed.
Mixed fracture	A part of the fracture occurs at the coating/metal interface, and a part of it occurs within the body of the coating. The peeling area of the coating is smaller than the loading area.
Normal fracture	The fracture occurs within the body of the coating, and the peeling area of the coating is equal to the loading area.
Failure fracture	The fracture occurs at the interface between the coating and the substrate, and the peeling area is larger than the loading area.

Figure 16 shows that the fracture morphology of the epoxy varnish coating and the 35 wt% mica/epoxy coating before immersion (0 h) were of the cohesive fracturing type, indicating that the two coatings had good adhesion before the immersion test. After immersion for 60 h, the fracture morphology of the epoxy varnish coating changed into mixed fracturing. Based on the above results, the solution began to penetrate into the coating/metal interface, and the adhesion of the coating decreased, but the coating still had good protective performance. However, the fracture morphology of the 35 wt% mica/epoxy coating was still cohesive fracturing, indicating that the electrolyte had not penetrated into the coating/metal interface, which was consistent with the above studies.

After immersion for 120 h, the cross-sectional morphology of the epoxy varnish coating became a normal fracture. This might be due to the constant infiltration of the electrolyte, which destroy the adhesion between the coating and the metal interface, resulting in a continuous decline in adhesion. However, the fracture morphology of the 35 wt% mica/epoxy coating was a mixed fracture, indicating that the solution began to penetrate into the coating/metal interface.

After immersion for 240 h, the fracture morphology of the epoxy varnish coating was a failure fracture, and rust could be seen on the surface of the metal matrix, at which time the adhesion of the

coating was completely lost. The fracture of the 35 wt% mica/epoxy coating was a mixed fracture. By comparison, it was easy to see that the epoxy varnish coating fracture evolved from a cohesive fracture to a failure fracture with the extension of immersion time. However, the fracture morphology of the 35 wt% mica/epoxy coating changed from a cohesive fracture to a mixed fracture.

In summary, the main reason for the loss of coating protection was the loss of wet adhesion. Adding mica could slow the diffusion rate of the corrosive medium into the coating, improve the corrosion resistance of the coating and effectively change the corrosion resistance mechanism of the coating. Therefore, a reasonable selection of filler content could enhance the impermeability of the coating to corrosive media and extend the service life of the coating.

3.5.4 Corrosion resistance process

Figure 17 is a schematic diagram of the mica/epoxy coating with different contents of preventative media. When the epoxy resin and curing agent were crosslinked to form a coating, a certain number of pores were formed in the coating, which was beneficial to the infiltration of the corrosive medium into the coating.

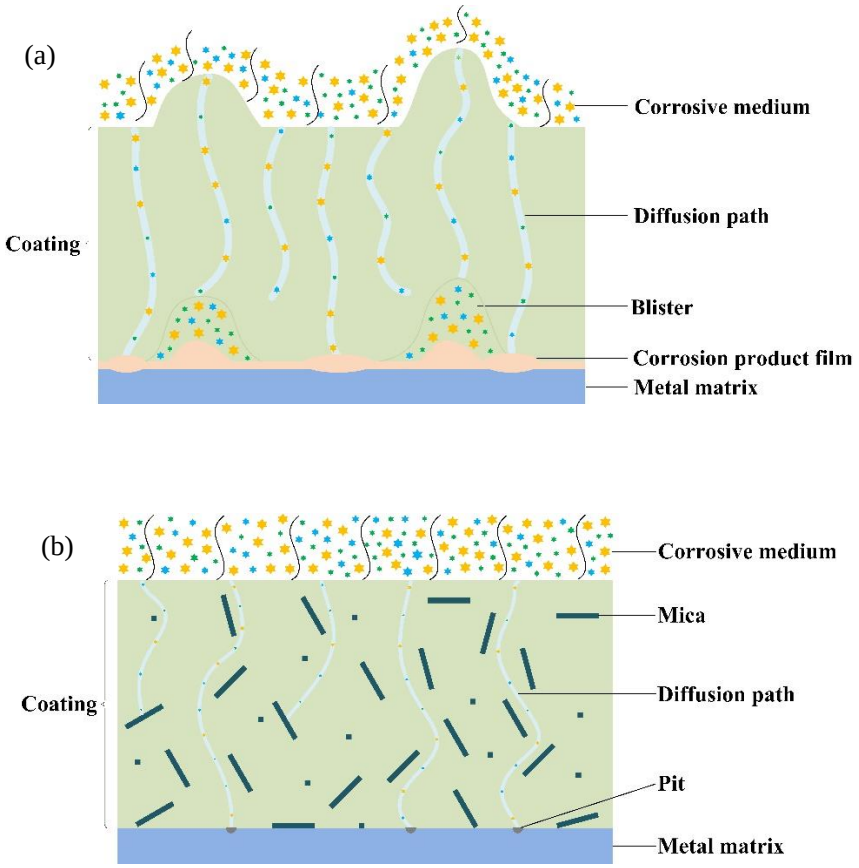

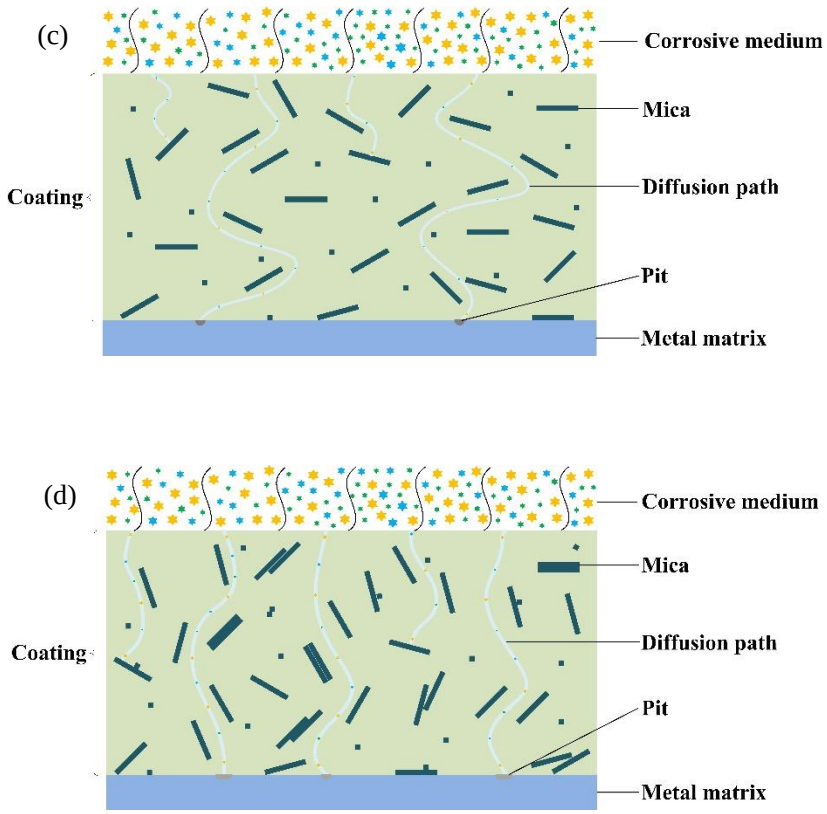

Figure 17. Corrosion products and coating debonding schematics of mica/epoxy coatings with different contents of barrier medium infiltrated at the interface. (a)=0 wt%, (b)＜35 wt%, (c)=35 wt%, (d)＞35 wt%.

At the beginning and end of the immersion experiment for the epoxy varnish coating, the corrosive medium penetrated the coating through channels to corrode the metal matrix, resulting in the weakening of adhesion between the coating and the metal matrix. The resistance value R_c of the epoxy varnish coating decreased from 6.956×10^7 Ω·cm^2 to 3.715×10^5 Ω·cm^2, which could be equivalent to a series relationship between R_c representing coating performance and the double electric layer circuit representing the electrochemical characteristics for metal corrosion in the impedance fitting circuit diagram, as shown in Figure 7(a). The self-corrosion potential E_{corr} decreased from -0.611 V to -0.821 V. The self-corrosion current I_{corr} increased from 2.25×10^{-10} A·cm^{-2} to 1.02×10^{-9} A·cm^{-2}. The polarization resistance R_p decreased from 9.04×10^6 Ω·cm^2 to 8.96×10^5 Ω·cm^2. The corrosion resistance of the epoxy varnish coating decreased gradually with increasing immersion time. With the extension of immersion time, more corrosion medium reached the interface, and the corrosion of the metal matrix intensified. Corrosion products accumulated at the connection between the inner channel of the coating and the matrix led to a decrease in adhesion between the coating and the metal matrix. As more of the metal matrix was exposed to the corrosive medium, corrosion became more severe. It formed a vicious cycle and led to the peeling, and ultimately, to the swelling of the epoxy varnish coating.

When mica of larger diameters and thicknesses was used to interlace in the coating, the resultant mica/epoxy coating formed a “labyrinth effect” [51] that increased the diffusion path of the corrosive medium in the coating and prolonged the time to the onset of corrosion in the corrosive

medium. The coating was divided into many blocks so that the expansion coefficient and shrinkage stress of the coating were improved, and the corrosion resistance and service life of the coating were also improved.

In this study, a surface modification to the mica was carried out before adding the mica to the epoxy resin, and it was found that the coupling agent KH-550 was successfully grafted onto the surface of the mica (organosilicon compound). This coupling agent easily bonded with the epoxy resin, so the mica had better compatibility with the epoxy resin, which greatly improved the dispersion of mica in the epoxy resin and the binding force between the mica and the epoxy resin [52]. To determine the performance conditions of the mica/epoxy coating, thermal stability tests were undertaken for the mica/epoxy coating and the epoxy varnish coating. The results showed that the thermal stability of the coating after adding mica was higher than that of the epoxy varnish coating. In other words, after adding mica, the epoxy coating was less affected by temperature and other factors, and the thermal stability of the mica/epoxy coating prepared with 35 wt% mica content performed the best.

Furthermore, it was found from the simulated immersion tests that there were fewer bubbles and cracks in the mica/epoxy coating than in the epoxy varnish coating, and there were no defects when the mica content was 35 wt%. Meanwhile, it was found that the contact angle of the mica/epoxy coating was slightly larger than that of the epoxy varnish coating, indicating that the wettability of the coating was slightly lower after adding mica, which made the transfer of the corrosive medium slower and slowed the corrosion effect on the metal matrix. In addition, the water absorption of the mica/epoxy coating was lower than that of the epoxy varnish coating, which had a strong shielding effect against the corrosive medium. According to the kinetics analysis for water absorption, the diffusion coefficient of the mica/epoxy coating decreased by an order of magnitude compared with that of the epoxy varnish coating, indicating that the addition of mica made the diffusion channels longer, it made the diffusion of the corrosive medium more difficult and it enhanced the corrosion resistance of the coating. This was consistent with previous research. After adding mica to the coating, E_{corr} increased, I_{corr} decreased, and corrosion resistance increased, indicating that the diffusion coefficient of the mica epoxy coating was positively correlated with E_{corr} and negatively correlated with I_{corr}.

Before the immersion tests, the adhesion of the epoxy varnish coating was greater than that of the mica/epoxy coating for all mica contents. As seen from Figure 11, a part of the mica appeared in the metal matrix, but the mica had no adhesion to the metal matrix, so the contact area between the epoxy coating and the metal matrix decreased and adhesion decreased. Before immersion and after immersion for 60 h and 120 h, the adhesion of the mica/epoxy coating decreased with increasing mica content. After immersion for 240 h, with increasing mica content, the adhesion first increased and then decreased, and the maximum value occurred when the mica content was 35 wt%. Subsequently, the adhesion fracture analysis of the epoxy varnish coating and the 35 wt% mica/epoxy coating showed that the mica/epoxy coating did not expose the metal matrix when the epoxy varnish coating peeled off. When the epoxy varnish coating broke, only a small area of the mica/epoxy coating fell off.

In summary, the addition of mica to an epoxy coating impedes the progress of the corrosion medium to the metal surface. The electrochemical tests showed that the resistance of the mica/epoxy coating was 1~2 orders of magnitude higher than that of the epoxy varnish coating at each immersion stage, the E_{corr} of the coating with mica was higher than that of the epoxy varnish coating, and the I_{corr}

was lower, indicating that its corrosion resistance was higher than that of the epoxy varnish coating. The addition of mica to the coating can greatly improve the corrosion resistance of the coating, but an appropriate amount of mica need to be added. When the amount of mica was less than 35 wt%, it could not effectively shield the metal from the corrosive medium. When the amount of mica was greater than 35 wt%, it was unevenly dispersed in the coating and exhibited aggregation adhesion, which increased the number of internal defects in the coating and weakened the corrosion resistance of the coating. Therefore, the mica/epoxy coating prepared by adding 35 wt% mica had the best protective performance.

4. CONCLUSIONS

(1) Compared with an epoxy varnish coating without mica, the addition of mica enhanced the mechanical properties, water absorption properties, and thermal stability of the protective coating. After adding 35 wt% mica to the epoxy varnish coating, its wet adhesion increased by 230%, impermeability increased by 98.5%, and thermal stability increased by 14.4%.

(2) Compared with an epoxy varnish coating without mica, mica addition enhanced the corrosion resistance of the protective coating. With increasing mica content, the protective performance of the coating first increased and then decreased; the protective performance of the mica/epoxy coating was the best when the mica content was 35 wt%. The corrosion resistance increased by 3 orders of magnitude.

(3) The addition of mica can improve the impermeability of the protective coating, increase the length of the path for medium infiltration into the coating, slow down the penetration of corrosive media, effectively inhibit the occurrence and development of coating/metal interface reactions, change the corrosion resistance mechanism of the coating, and prolong the service life of the anticorrosion coating.

ACKNOWLEDGEMENT

This research was supported by the National Key Research and Development Program of China (2019YFF0217500).

References

1. Aisha H. Al-Moubaraki, and I.B. Obot, *Arabian J. Chem*., 14 (2021) 103116.
2. B.R. Hou, X.G. Li, and X.M. Ma, C.W. Du, D.W. Zhang, M. Zheng, W.C. Xu, D.Z. Lu, and F.B. Ma, *npj Mater. Degrad.*, 1 (2017) 29-33.
3. Z.Q. Wang, Z.Y. Zhou, W.C. Xu, L.H. Yang, B.B. Zhang, and Y.T. Li, *Eng. Fail. Anal.*, 115 (2020) 104659.
4. X.L. Du, X.J. Dai, Z.C. Li, X.F. Du, H.B. Shi, J.Y. Wu, H. Lou, X. Feng, L. Zhao, and Z.N. Li, *Energy Rep*., 7 (2021) 1280-1292.
5. D.Y. Yang, Z.Y. Chen, X.S. Rong, H.Q. Zhang, and F.X. Qiu, *J. Polym. Res.*, 21 (1) (2014) 1-8.
6. T. Wan, T.S. Zang, R. Zhang, and X.C. Sun, *Mater. Sci. Ed.*, 27 (3) (2012) 437-442.
7. J.D. Oliveira, R. C. Rocha, and A. G. de Sousa Galdino, *J. Mater. Res.* Technol., 8 (2) (2019) 1729-1736.
8. Nivin M. Ahmed, Walaa M. Abd El-Gawad, Ahmed A. El_Shami, and Eglal M.R. Souaya, *Pigm. Resin Technol.*, 46 (3) (2017) 181-193.

9. C.F. Yang, W.H. Smyrl, and E.L. Cussler, *J. Membr. Sci.*, 231 (1) (2003) 1-12.
10. L. Lapčík, D. Maňas, B. Lapčíková, M. Vašina, M. Staněk, K. Čépe, J. Vlček, K.E. Waters, R.W. Greenwood, and N.A. Rowson, *Compos. Part B*., 141(2018) 92-99.
11. F.T. Shirehjini, I. Danaee, H. Eskandari, and D. Zarei, *J. Mater. Sci. Technol.*, 32 (11) (2016) 1152-1160.
12. A. Ghasemi-Kahrizsangi, H. Shariatpanahi, J. Neshati, and E. Akbarinezhad, *Appl. Surf. Sci.*, 331 (2015) 115-126.
13. F.D. Meng, L. Liu, W.L. Tian, H. Wu, Y. Li, T. Zhang, and F.H. Wang, *Corros.* Sci., 101 (2015) 139-154.
14. M. Yadav, T.K. Sarkar, and T. Purkait, *J. Mater. Eng. Perform.,* 24 (12) (2015) 4975-4984.
15. M. Yadav, T. K. Sarkar, and T. Purkait, *J. Mol. Liq*., 212 (2015) 731-738.
16. R. Ding, X. Wang, J.M. Jiang, T.J. Gui, W.H. Li, *J. Mater. Eng. Perform.*, 26 (7) (2017) 3319-3335.
17. M. N. Prabhakar, G. M. Raghavendra, B.V.D. Vijaykumar, K. Patil, J. Seo, and S. Jung-il, *Cellul.*, 26 (16) (2019) 8801-8812.
18. C.H. Chang, T.C. Huang, C.W. Peng, T.C. Yeh, H.I. Lu, W.I. Hung, C.J. Weng, T.I. Yang, and J.M. Yeh, *Carbon*., 50 (14) (2012) 5044-5051.
19. L.A.Al Juhaiman, A.A. Aljaghwani, W.K. Mekhamer, *Int. J. Electrochem.* Sci., 15 (2020) 6938-6954.
20. S.J. Peng, *Guangzhou Chem. Ind. (in China)*, 42 (21) (2014) 91-92+98.
21. P. Gao, and X.X. Xue, *Mater. Prot. (in China)*, 44 (03) (2011) 47-49+53+90.
22. Bhaskaran, P. D. Pancharatna, S. Lata, and G. Singh, *J. Mol. Liq.*, 278(2019) 467.
23. F.D. Meng, *Harbin: Harbin Engineering University (in China)*, 2013.
24. X.D. Ren, H. Wang, Q. Wei, Y. Lu, B.W. Xiao, and J. Xie, *Corros. Sci.*, 189(2021) 109619.
25. S. Liu, Y. Gu, S.L. Wang, Y. Zhang, Y.F. Fang, D.M. Johnson, and Y.P. Huang, *Chin. Sci. Bull.*, 58 (19) (2013) 2340-2346.
26. L. Gu, X. Zhao, X. Tong, J. Ma, B. Chen, S. Liu, H.C. Zhao, H.B. Yu, and J.M. Chen, *Int. J. Electrochem. Sci.*, 11 (2016) 1621-1631.
27. S. Liu, L. Gu, H.C. Zhao, J.M. Chen, and H.B. Yu, *J. Mater. Sci. Technol.*, 32 (5) (2016) 425-431.
28. S.R. Wang, J.W. Yang, J.P. Cao, L.J. Gao, and C.X. Yan, *Int. J. Electrochem. Sci.*, 14 (2019) 9671-9681.
29. C. Shi, Y.W. Shao, Y.Q. Wang, G.Z. Meng, and B. Liu, *Prog. Org. Coat.*, 117(2018) 102-117.
30. B.J. Dou, Y.Q. Wang, T. Zhang, B. Liu, Y.W. Shao, G.Z. Meng, and F.H. Wang, *J. Electrochem. Soc.*, 163 (2016) C917-927.
31. B. Faryad, J. Mehdi, P. Mahmoud, K. Amirreza, and T. Morteza, *Int. J. Press. Vessels Pip.*, 193(2021) 104470.
32. D. Zhang, H.Q. Zhang, S. Zhao, Z.G. Li, and S.X. Hou, *Int. J. Electrochem. Sci.*, 14 (2019) 4659-4667.
33. S. Fazli-Shokouhi, F. Nasirpouri, and M. Khatamian, *J. Coat. Technol. Res*., 16 (4) (2019) 983-997.
34. Y. Zhao, J.Q. Ma, K. Chen, C.D. Zhang, C. Yao, S.X. Zuo, and Y. Kong, *Nano*, 12 (5) (2017) 1750056.
35. Q.B. Yang, Y. He, Y. Fan, Y.Q. Zhan, Y. Tang, *Int. J. Electrochem. Sci.*, 11 (2016) 5103-5110.
36. R.A. Shakoor, U.S. Waware, R. Kahraman, A. Popelka, and M.M. Yusuf, *Int. J. Electrochem. Sci.*, 12 (2017) 4384-4391.
37. X.Q. Fu, X.X. Shi, S.L. Duan, M.Q. Shen, J.R. Lin, and M.J. Jiang, *Int. J. Electrochem. Sci.*, 15 (2020) 6448-6463.
38. H.T. Wang, J.R. Wang, M.D. Ger, and K.H. Hou, *Int. J. Electrochem. Sci.*, 11 (2016) 2419-2432.
39. Y.S. Hao, F.C. Liu, E.H. Han, S. Anjum, and G.B. Xu, *Corros. Sci.*, 69 (2013) 77-86.
40. Y. Cubides, and H. Castaneda. *Corros. Sci.,* 109 (2016) 145-161.
41. H.Y. Xu, B. Li, X. Han, Y. Wang, X.R. Zhang, and S. Komarneni, *J. Appl. Polym. Sci.*, 136 (21) (2019) 47562.

42. Y. Liu, G.L. Lu, J.D. Liu, Z.W. Han, and Z.N. Liu, *Appl. Surf. Sci.*, 264 (2013) 527-532.
43. S.V. Gnedenkov, S.L. Sinebryukhov, V.S. Egorkin, D.V. Mashtalyar, D.A. Alpysbaeva, and L.B. Boinovich, *Colloids Surf., A.*, 383 (1) (2011) 61-66.
44. C. Perez, A. Collazo, M. Izquierdo, P. Merino, and X.R. Novoa, *Prog. Org. Coat.*, 36 (1) (1999) 102-108.
45. C. Pérez, A. Collazo, M. Izquierdo, P. Merino, and X.R. Nóvoa, *Prog. Org. Coat.*, 37 (3) (1999) 169-177.
46. Z. Kolek, *Prog. Org. Coat*., 30 (4) (1997) 287-292.
47. J.T. Zhang, J.M. Hu, J.Q. Zhang, and C.N. Cao, *Prog. Org. Coat.*, 49 (4) (2004) 293-301.
48. J.T. Zhang, J.M. Hu, J.Q. Zhang, and C.N. Cao, *Prog. Org. Coat.*, 51 (2) (2004) 145-151.
49. J.A. Yan, Z.M. Gao, J. Song, Z.H. Liu, and Q.C. Tan, *Int. J. Electrochem. Sci.*, 15 (2020) 10253-10261.
50. J.Y. Li, X.R. Li, K. Zhu, H.H. Wang, and G.Q. Fei, *J. Macromol. Sci., Part A: Pure Appl. Chem.*, 55 (9) (2018) 649-657.
51. Z.H. Chen, C. He, F. Yu, and Y. Wang, *Int. J. Electrochem. Sci.*, 12 (2017) 2798-2812.
52. J.P. Zhuang, and K.K. Du, *Henan Chem. Ind. (in China)*, 28 (12) (2011) 28-30.

© 2022 The Authors. Published by ESG (www.electrochemsci.org). This article is an open access article distributed under the terms and conditions of the Creative Commons Attribution license (http://creativecommons.org/licenses/by/4.0/).